Effect of Calcination Process on Synthesis of Ceria Particles, and Its Influence on Shallow Trench Isolation Chemical Mechanical Planarization Performance

Japanese Journal of Applied Physics
Vol. 45, No. 6A, 2006, pp. 4893–4897

Effect of Calcination Process on Synthesis of Ceria Particles, and Its Influence on Shallow Trench Isolation Chemical Mechanical Planarization Performance

Dae-Hyeong KIM, Hyun-Goo KANG[1], Sang-Kyun KIM[2], Ungyu PAIK[2] and Jea-Gun PARK[1*]

KCTech, 271-14 Kyeruk-Ri, Miyang-Myon, Anseong-Si, Kyongki-Do, Korea
[1]*Nano-SOI Process Laboratory, Hanyang University, 17 Haengdang-Dong, Seoungdong-Gu, Seoul 133-791, Korea*
[2]*Department of Ceramic Engineering, Hanyang University, 17 Haengdang-Dong, Seoungdong-Gu, Seoul 133-791, Korea*

(Received October 1, 2005; accepted February 23, 2006; published online June 8, 2006)

The effect of the calcination process for cerium carbonate, a precursor of ceria, on the degree of synthesis and colloidal properties of ceria particles in aqueous media, which greatly influence shallow trench isolation (STI) chemical mechanical planarization (CMP) performance, was investigated. A two-step calcination process, consisting of decarbonation and crystal growth, resulted in a higher degree of synthesis for the same crystal size, a narrower particle size distribution, and better dispersion of the ceria particles, than conventional one-step calcination. These properties enhanced certain aspects of STI CMP performance, leading to a higher oxide removal rate, a better selectivity between oxide and nitride, and fewer defects, including remaining particles. [DOI: 10.1143/JJAP.45.4893]

KEYWORDS: calcination, density, particle size distribution, agglomeration, ceria, slurry, STI CMP

1. Introduction

The shallow trench isolation (STI) process is one of the most crucial applications of chemical mechanical planarization (CMP) technologies. It has replaced the local oxidation of silicon (LOCOS) method, providing a high degree of planarity necessary to meet stringent photolithography requirements. In STI CMP, the selectivity between oxide and nitride layers is a critical factor determining the STI process margin and product yield.[1–4] At the same time, a high oxide removal rate is necessary for a high production efficiency. Recently, therefore, ceria slurry has been widely used in STI CMP.[5] Ceria slurry, however, has a major disadvantage in that it produces many kinds of defect, including micro scratches, caused by large grains and agglomerated particles.[6–10] Therefore, to improve STI CMP using ceria slurry, it is necessary to minimize the production of large grains and agglomeration of particles, while maintaining a high oxide removal rate and good selectivity.

Recently, the physical properties of ceria particles and their polishing mechanism have been investigated.[11] Few studies, however, have examined the effect of the calcination of cerium carbonate, which is used as a precursor for ceria particles, on STI CMP performance, even though the calcination process determines important characteristics of both ceria particles and slurry. The degree of synthesis affects removal rate and selectivity. The size distribution of ceria particles and their agglomeration behavior greatly influence the remaining particles and micro scratch count on oxide films. In this study, therefore, we analyzed the characteristics of two kinds of ceria particle manufactured by different calcination processes, namely, the conventional one-step calcination and a two-step calcination consisting of decarbonation and crystal growth. In addition, STI CMP performance was compared between the two processes.

2. Experimental Procedure

In this study, two kinds of ceria particle were synthesized from a starting material of high-purity cerium carbonate by the solid-state displacement reaction method. The calcination generated a yellowish-white ceria powder. One kind of ceria powder, denoted as sample A, was calcined by the conventional one-step calcination method while the other, sample B, was calcined by the two-step calcination method. In the case of one-step calcination, the carbonate precursor was calcined at 700 °C for 4 h only once. In two-step calcination, on the other hand, ceria particles were obtained after a second step of calcination at 650 °C for 4 h, after the initial calcination at 650 °C for 4 h. In addition, between the first and second steps of calcination, ceria particles were pulverized with a dry mechanical crusher called the air jet mill. Figures 1(a) and 1(b) show ceria particles before and after the dry mechanical crushing, respectively. That is, sample B was calcined for a longer period and at a lower temperature than sample A. Furthermore, ceria particles of sample B were well calcined even at the center of agglomerated large particle shown in Fig. 1(a) by the second step of calcination carried out after the dry mechanical crushing, while those of sample A were not, since the core part of agglomerated particles was pulled apart during the dry pulverization. After the calcination of samples A and B, ceria powders were pulverized by wet mechanical milling for 6 h to reduce their secondary particle size to the target size of 250 nm, and to disperse the particles in an aqueous medium after mixing them with de-ionized water and commercially available anionic acrylic polymers as a dispersant.

The average crystallite size of ceria particles was measured by X-ray diffraction (XRD; RINT/DMAX-2500, Rigaku, Japan), with calculation using the Debye–Scherer equation. The density of the powder was measured with a pycnometer (Accupyc 1330, Micromeritics, U.S.A.), and porosity was calculated from density data using the following equation:

$$\text{Porosity} = [(N_t - N_m)/N_t] \times 100,$$

where N_t and N_m denote the theoretical density and the measured density, respectively. The theoretical density of ceria particles was taken as 7.2 g/cm^3. The size of individual grains was also observed by transmission electron microscopy (TEM; JEM-2010, JEOL, Japan). To investigate the

*E-mail address: parkjgL@hanyang.ac.kr

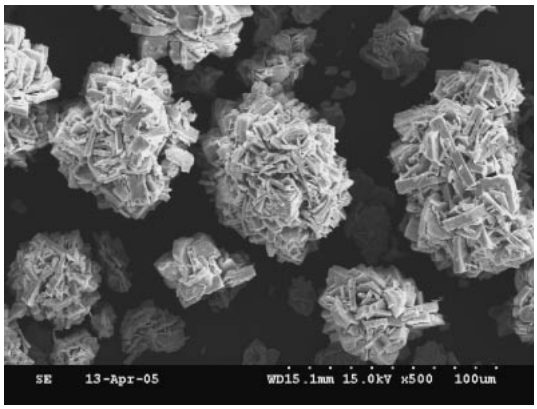

(a)

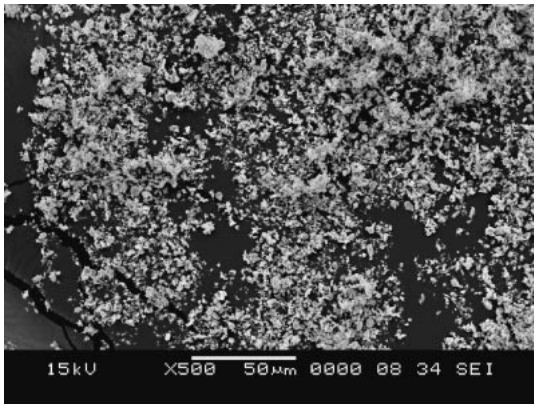

(b)

Fig. 1. SEM images of ceria particles for sample B: (a) after first step of calcination but before dry mechanical crushing and (b) after dry mechanical crushing of ceria particles calcined at first step.

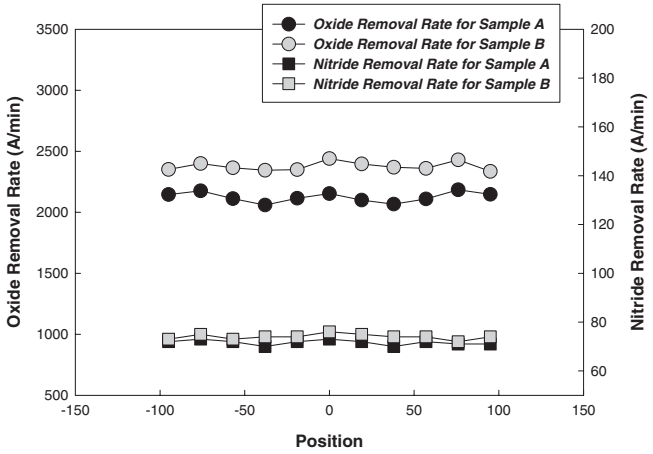

(a)

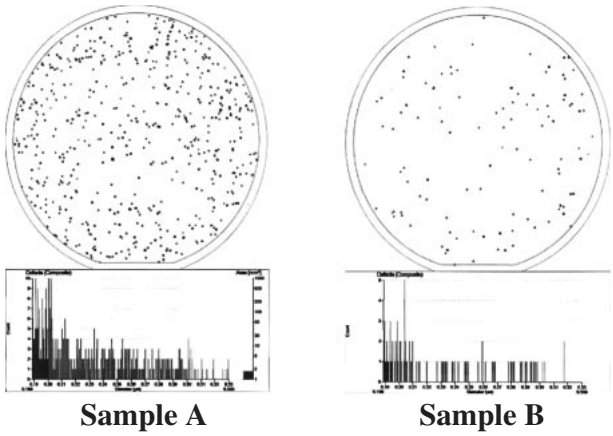

(b)

Fig. 2. STI CMP test results: (a) oxide and nitride removal rates and (b) map of the remaining particles on oxide film.

agglomeration behavior of ceria particles in the aqueous medium, we used a particle size analyzer (LA-910, HORIBA, Japan) equipped with an ultrasonic device, which can be applied to break agglomerated particles by cavitation. Particle size was measured with and without ultrasonic treatment, and the difference between particle size measurements was calculated as a measure of the degree of agglomeration.[12] To quantify the extent of agglomeration, we defined the following parameter:

$$\mathrm{dD50} = \mathrm{D50\ without\ ultrasonic\ treatment} - \mathrm{D50\ with\ ultrasonic\ treatment},$$

where D50 denotes the median of particle size distribution, and a large dD50 means large aggregated particles.

To investigate the influence of the calcination process on STI CMP performance, CMP evaluation tests were carried out using two different ceria slurries and commercial 8 in. wafers with plasma-enhanced tetraethylorthosilicate (PE-TEOS) or low-pressure chemical-vapor-deposited (LPCVD) nitride films. The thicknesses of the as-deposited oxide and nitride films were 7000 and 1500 Å, respectively. A CMP machine for 8 in. wafers (6EC, Strasbaugh, U.S.A.) with a grooved IC1000/Suba IV pad (Rodel, USA) was used. The rotation speeds of the head and the table were both 70 rpm, the relative velocity between the pad and wafer was 250 fpm (feet per min), and the slurry flow rate was 100 cm^3/min. To calculate removal rate, film thickness was measured with Nanospec 180 (Nano-metrics, U.S.A.). The number of remaining particles larger than 0.2 μm was determined using the stationary beam technology and optional bright field channel of a Surfscan SP1 (KLA-Tencor, U.S.A.).

3. Results and Discussion

As shown in Fig. 2, sample B showed better CMP performance, including a higher oxide removal rate, better selectivity, and fewer remaining particles on the oxide film. Since the slurry containing more remaining particles usually causes more microscratches, it can be expected that sample A has more microscratches.[10,13] These results are summarized in Table I. Oxide removal rate usually depends on particle sizes, namely, grain size and secondary particle size. As these particle sizes increase, oxide removal rate also increases, while nitride removal rate remains almost the same if the concentration of the additive is above a critical point.[14–16] However, the average grain size calculated from XRD data and the secondary particle size measured by the conventional light scattering method with ultrasonic treatment were similar for samples A and B, indicating no size effect on removal rate, as shown in Table II. There was a difference, on the other hand, in the density and porosity of ceria particles. As summarized in Table III, the density of

Table I. Summary of CMP test results.

Item	Oxide removal rate (Å/min)	Nitride removal rate (Å/min)	Selectivity	Particle count on oxide film (larger than 0.2 μm)
Sample A	2120	72	29	516
Sample B	2376	74	32	111

Table II. Summary of particle sizes.

Item	Grain size (nm)	Secondary particle size with ultrasonic treatment (nm)	Secondary particle size without ultrasonic treatment (nm)	dD50 (nm)
Sample A	25.5	249	336	87
Sample B	25.1	251	252	1

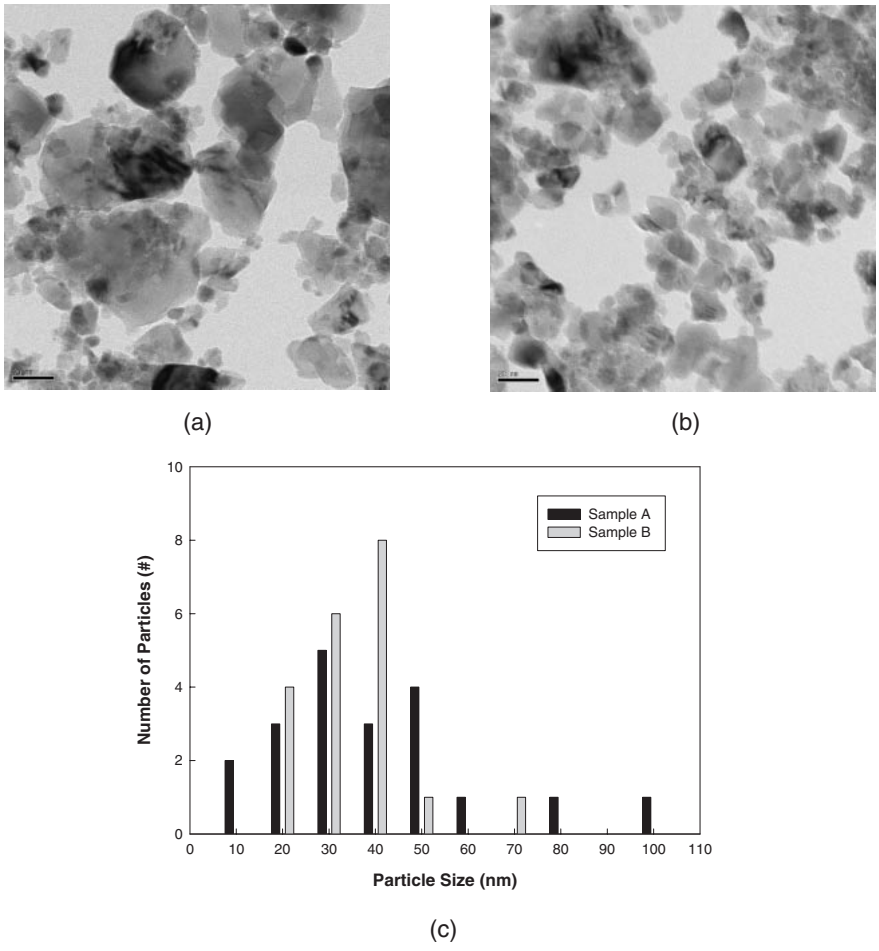

Fig. 3. TEM images of ceria slurries formed using samples A and B and grain size distribution analyzed from TEM images: (a) sample A, ×100 K; (b) sample B, ×100 K; and (c) grain size distribution.

Table III. Density and porosity.

Item	Measured density (g/cm^3)	Theoretical density (g/cm^3)	Porosity (%)
Sample A	5.9	7.2	18.2
Sample B	6.2	7.2	13.8

sample B was higher than that of sample A, while porosity exhibited the opposite tendency. This means that ceria particles of sample B were denser and harder (less porous) owing to the higher degree of synthesis than those of sample A, resulting in a higher oxide removal rate. Moreover, the nitride removal rates were very similar, which means better selectivity for sample B than for sample A. In STI CMP, ceria particles penetrate the viscous layer on the oxide or nitride film, react with the hydrated surface to form covalent bonds such as Ce–O–Si, and then detach lumps of oxide and nitride.[17] The viscous layer on the nitride film, however, is too thick for a difference in the degree of synthesis to be detected in terms of nitride removal rate.[18,19]

To determine the reason for the difference in the count of

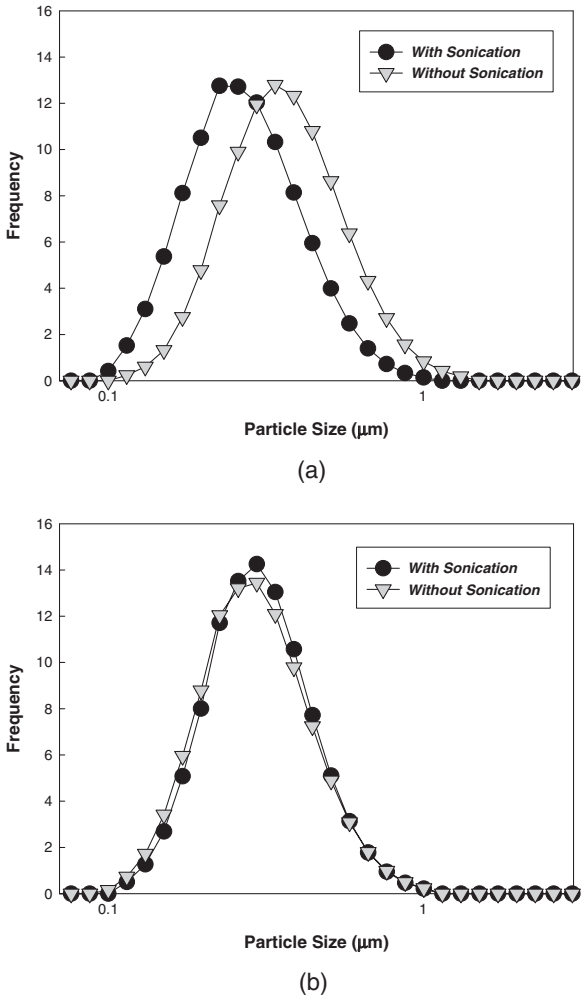

Fig. 4. Difference between particle sizes with and without ultrasonic treatment: (a) sample A and (b) sample B.

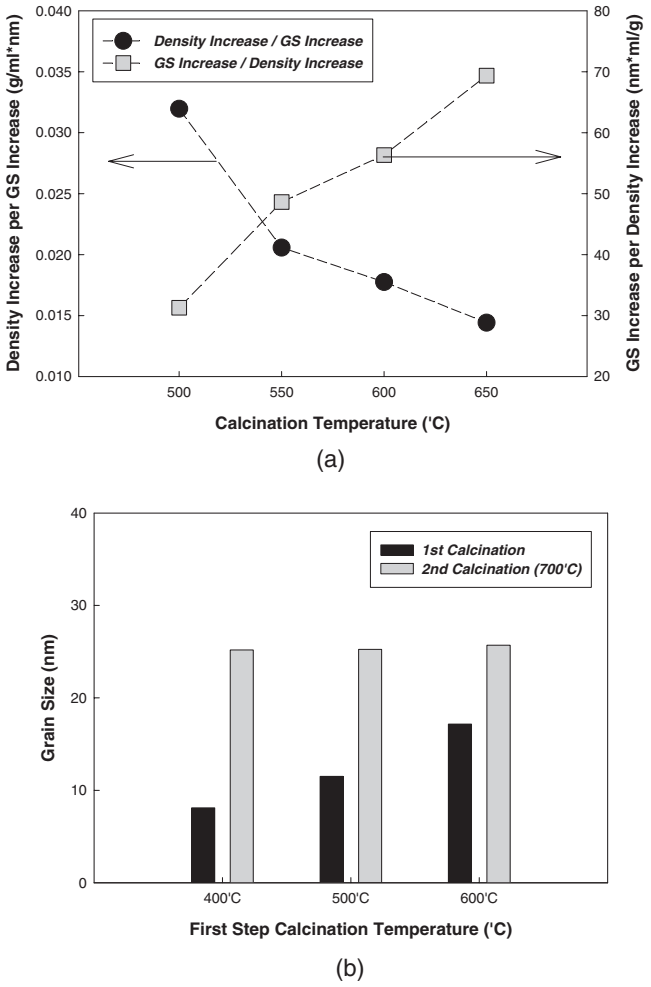

Fig. 5. Density and grain size measured by XRD: (a) efficiencies of decarbonation and crystal growth at various calcination temperatures and (b) grain sizes calculated from XRD data for first and second calcination steps.

remaining particle on the oxide film between samples A and B, grain size distribution was analyzed by TEM, as shown in Figs. 3(a) and 3(b). Sample A contained both large and small grains, while sample B was composed of uniformly distributed and medium-sized particles. The size distribution of 20 particles randomly selected from the TEM images is shown in Fig. 3(c). As confirmed by the TEM images, sample A had a wider size distribution than sample B. In particular, the large grains of sample A led to defects, including remaining particles. In addition, the agglomeration behavior of sample slurries was measured using a particle size analyzer, as shown in Fig. 4 and Table II. The difference in particle size between the measurements with and without ultrasonic treatment was much larger for sample A than for sample B, indicating that sample A had greater agglomeration. This was attributed to the broad size distribution of small and large particles in sample A, as shown in TEM images. Small particles with large surface areas aggregate around large particles so as to reduce the total surface energy, thus promoting agglomeration.[20)]

These differences between samples A and B in terms of density, porosity and grain size distribution, which led to differences in STI CMP performance, were attributed to the difference in the two calcination processes, in which cerium carbonate reacts with oxygen via the following reaction:[21)]

$$CeCO_3OH + 1/4\ O_2 \rightarrow CeO_2 + CO_2 + 1/2\ H_2O.$$

According to Kosynkin *et al.*, the oxidation reaction of the carbonate precursor, consisting of decarbonation and crystal growth, is not always completed at a specific temperature range, and the efficiency of decarbonation of the carbonate precursor and that of the crystal growth of ceria particles are different in terms of the temperature range.[22)] In a lower temperature range between 400 and 500 °C, the efficiency of decarbonation is high, while the crystal growth rate is low. In a higher temperature range between 700 and 800 °C, however, the relationship between decarbonation efficiency and crystal growth rate is reversed, namely, slow decarbonation and fast crystal growth.[22)] Therefore, during calcination at the low-temperature range, density increases rapidly while grain size increases slowly, since most of the energy is used not for crystal growth but for decarbonation. During the calcination at high temperature range, on the other hand, the grain size increases rapidly, since the grains combine with each other to stabilize themselves by reducing the total surface energy. Figure 5(a) shows these variations, as represented through a comparison between the increase in density per unit increase in grain size and the increase in grain size per unit increase in density at various temperatures. As a consequence, sample A, which was calcined at a

high temperature, had more large grains than sample B, and the density of sample A was lower than that of sample B, which was calcined for a long period at a low temperature.

In addition, the core part of large agglomerated particles shown in Fig. 1(a) reacts more slowly than the outer part of particles and thus cannot be calcined completely. This phenomenon is due to both a low supply of reactant oxygen and difficulty in removing the carbon dioxide product. The large agglomeration of particles results in the large mass-transfer resistance of gases, which prevents those gases from diffusing inside or outside of agglomerated particles.[23,24] Therefore, as confirmed in the above equation of calcination reaction, such a slow diffusion and mass transfer of gases retard the calcination reaction, resulting in small grains in the core part. In the case of sample B, however, the core part can also be well calcined since the dry mechanical crushing before the second step of calcination pulls the core part out of agglomerated particles. Such complete calcination removes small grains observed in sample A, which was prepared by the one-step calcination method. Moreover, in the second step of calcination, the size of small grains increased much faster than that of large grains. As shown in Fig. 5(b), when ceria powders processed with the first step of calcination at 400, 500, and 600 °C, and calcined with the second step at 700 °C, the final grain sizes calculated from the XRD data for the three samples were very similar at 25–26 nm. This happened even though the grain sizes after the first step were different, namely, 8.1 nm (400 °C), 11.5 nm (500 °C), and 17.2 nm (600 °C). Therefore, the additional crystal growth of large grains was restricted in the second step of calcination, even though active crystal growth of small grains occurred, resulting in narrow grain size distribution.

4. Conclusions

In this study, we have demonstrated that the two-step calcination method, in which ceria particles were well calcined to the core part of agglomerated precursor carbonate at low temperature for a long period, leads to ceria particles with a high density, a low porosity and a narrow size distribution, as observed in the case of sample B. By using the two-step calcination method, it is thus possible to generate dense particles with a higher degree of synthesis, without large grains causing micro-scratches and small grains triggering the agglomeration of colloidal particles. By using ceria particles calcined by the two-step method, we can improve STI CMP performance, with a higher oxide removal rate, a higher oxide-to-nitride selectivity, and fewer defects.

Acknowledgement

The Korea Ministry of Science and Technology supported this work through the National Research Laboratory (NRL) program. We thank Sumitomo Mitsubishi Silicon Corp. and Hynix Semiconductor, Inc. for helping us with our experiments.

1) H. Nojo, M. Kodera and R. Nakata: Proc. IEEE, San Francisco, CA, 1996, p. 349.
2) K. Hirai, H. Ohtsuki, T. Ashizawa and Y. Kurata: Hitachi Chemical Tech. Rep. No. 35, 2000, p. 17.
3) Y. Tateyama, T. Hirano, T. Ono, N. Miyashita and T. Yoda: Proc. Int. Symp. Chemical Mechanical Planarization IV, 2000, p. 297.
4) S. K. Kim, U. Paik, S. G. Oh, Y. K. Park, T. Katoh and J. G. Park: Jpn. J. Appl. Phys. **42** (2003) 1227.
5) J. P. Kim, U. Paik and J. G. Park: J. Korean Phys. Soc. **39** (2000) 197.
6) T. Detzel, S. Hosali, A. Sethuraman, J. F. Wang and L. Cook: Proc. CMP-MIC Conf., 1997, p. 202.
7) G. B. Basim, J. J. Adler, U. Mahajan, R. K. Singh and B. M. Moudgil: J. Electrochem. Soc. **147** (2000) 3523.
8) R. K. Singh, S. M. Lee, K. S. Choi, G. B. Basim, W. Choi, Z. Chen and B. M. Moudgil: Mater Res. Bull. **27** (2002) 752.
9) T. L. Neo, E. S. Y. Shang and C. M. Chong: Proc. Int. Symp. Semiconductor Manufacturing, 2001, p. 321.
10) Y. J. Seo, G. U. Kim and W. S. Lee: Microelectron. Eng. **71** (2004) 209.
11) S. H. Lee, Z. Lu, S. V. Babu and E. Matijevi: J. Mater. Res. **17** (2002) 2744.
12) B. Pacaud, T. K. Doy, Y. Sasakawa and E. Rohart: unpublished.
13) K. Devriendt, P. Mertens, W. Fyen, K. Kenis, M. Schaekers, D. Guidoux, G. Sergeant, S. Robic and R. Moirin: Yield Manage. Solutions **3** (2000) 72.
14) H. G. Kang, T. Katoh, S. J. Kim, U. Paik, H. S. Park and J. G. Park: Jpn. J. Appl. Phys. **43** (2004) 365.
15) T. Katoh, H. G. Kang, U. Paik and J. G. Park: Jpn. J. Appl. Phys. **42** (2003) 1150.
16) S. K. Kim, P. W. Yoon, U. Paik, T. Katoh and J. G. Park: Jpn. J. Appl. Phys. **43** (2004) 7427.
17) T. Hoshino, Y. Kurata, Y. Terasaki and K. Susa: J. Non-Cryst. Solids **283** (2001) 129.
18) J. G. Park, T. Katoh, W. M. Lee, H. Jeon and U. Paik: Jpn. J. Appl. Phys. **42** (2003) 5420.
19) H. G. Kang, T. Katoh, M. Y. Lee, H. S. Park, U. Paik and J. G. Park: Jpn. J. Appl. Phys. **43** (2004) L1060.
20) H. Kamiya, M. Mitsui, H. Takano and S. Miyazawa: J. Am. Ceram. Soc. **83** (2000) 287.
21) C. H. Lu and H. C. Wang: Mater. Sci. Eng. B **90** (2002) 138.
22) V. D. Kosynkin, A. A. Arzgatkina, E. N. Ivanov, M. G. Chtoutsa, A. I. Grabko, A. V. Kardapolov and N. A. Sysina: J. Alloys Compd. **303–304** (2000) 421.
23) O. Levenspiel: *Chemical Reaction Engineering* (Wiely, New York, 1999) 3rd ed., Chap. 18, p. 378.
24) I. Ar and G. Dogu: Chem. Eng. J. **83** (2001) 131.